Applied Physics Letters

Equilibrium analysis of Mott memristor reveals criterion for negative differential resistance

Cite as: Appl. Phys. Lett. **118**, 223505 (2021); https://doi.org/10.1063/5.0049115
Submitted: 01 March 2021 . Accepted: 19 May 2021 . Published Online: 03 June 2021

Stephen A. Sarles, Joseph P. Wright, and Jin-Song Pei

AIP Publishing

Applied Physics Letters ARTICLE scitation.org/journal/apl

Equilibrium analysis of Mott memristor reveals criterion for negative differential resistance

Cite as: Appl. Phys. Lett. **118**, 223505 (2021); doi: 10.1063/5.0049115
Submitted: 1 March 2021 · Accepted: 19 May 2021 ·
Published Online: 3 June 2021

View Online Export Citation CrossMark

Stephen A. Sarles,[1,a)] Joseph P. Wright,[2] and Jin-Song Pei[3]

AFFILIATIONS

[1]Department of Mechanical, Aerospace, and Biomedical Engineering, University of Tennessee, Knoxville, Tennessee 37996, USA
[2]Division of Applied Science, Weidlinger Associates Inc., New York, New York 10005, USA
[3]School of Civil Engineering and Environmental Science, School of Electrical and Computer Engineering, University of Oklahoma, Norman, Oklahoma 73019, USA

[a)]Author to whom correspondence should be addressed: ssarles@utk.edu

ABSTRACT

Two-terminal electronic devices that exhibit voltage-controlled threshold switching (TS) via negative differential resistance (NDR) are important for many emerging applications. Pickett and Williams developed what has become a well-known physics-based model for nanoscale devices exhibiting NDR due to a reversible insulator-metal phase (Mott) transition. The Mott memristor model couples changes in electrical resistance and Joule heating to the phase of the material using one dynamic state variable, u, that describes the volume fraction of metal in the cross section of the device. The model formulation involves one nonlinear first-order ordinary differential equation and eight physical parameters. New equilibrium analysis reveals a simple condition that determines whether the model predicts NDR required for current–voltage (i–v) hysteresis in a voltage-controlled operation. We show that S-shaped NDR (also called current-controlled NDR) arises only above a critical ratio, M_c, of insulator to metal resistivity. Specifically, hysteresis in the i–v plane cannot occur below $M_c = e^2 + 1 \approx 8.39$ (i.e., $e \approx 2.718\ldots$; Euler's number), but above this value hysteresis appears. This understanding enables tuning of hysteretic features, including threshold voltages for resistive switching, which benefit the use of TS memristors as memory storage elements, as well as excitable devices mimicking neural action potentials.

Two-terminal, threshold switching (TS) devices built from transition metal oxides (e.g., VO_2, NbO_2, TiO_2) have attracted significant interest in recent years.[1–14] As Fig. 1 illustrates, these locally active[15] devices exhibit rapid increases in conductivity when an applied voltage surpasses a threshold, v_{on}. The conductive state remains until the voltage drops below a lower threshold, v_{off}. This behavior establishes a hysteretic, quasi-static current–voltage (i–v) curve when operated in a voltage-controlled mode.

TS devices are promising for use in many emerging applications, including as selectors in memristor crossbar arrays[1,14,16,17] and as leaky integrate-and-fire neurons and lossless neuristor circuits[13,18–20] due to the fact that TS can induce periodic[2,7,9–11] and chaotic[21] oscillations for efficient brain-like computing.[2,13,22,23] The observed i–v behavior in these devices is called S-shaped or current-controlled negative differential resistance (CC-NDR). The volatile nature of the increased conductance state at voltages between v_{off} and v_{on} distinguishes TS devices from nonvolatile memristors (i.e., resistive switching (RS) devices), which maintain their increased conductance state even when power is removed, and it is key in the use of TS devices in spike generating artificial neurons.

Pickett and Williams developed a coupled electro-thermal physical model that accurately captured the S-shaped CC-NDR that governs the steady-state i–v relationships and dynamic switching features observed in nanoscale NbO_2.[14] Their model considers that the change in conductance is the result of a Joule-heating induced Mott transition at a critical temperature within the material, switching it from an insulating oxide to conductive metal phase. Moreover, it was constructed within the framework of Chua's theory for memristance[24–26] using a dynamic state variable, u, that describes the volume fraction of metal in the cross section of the nanoscale device, which varies as a function of temperature and electrical power.

New understanding clarifies that S-shaped CC-NDR in NbO_2 is caused not only by a Mott insulator-metal transition (IMT) at temperatures of 1000 K, but also, rather, by a temperature-dependent nonlinear material conductivity $\sim < 500$ K described by Frenkel–Poole conduction.[4,5] Nonetheless, this physical model for IMT continues to

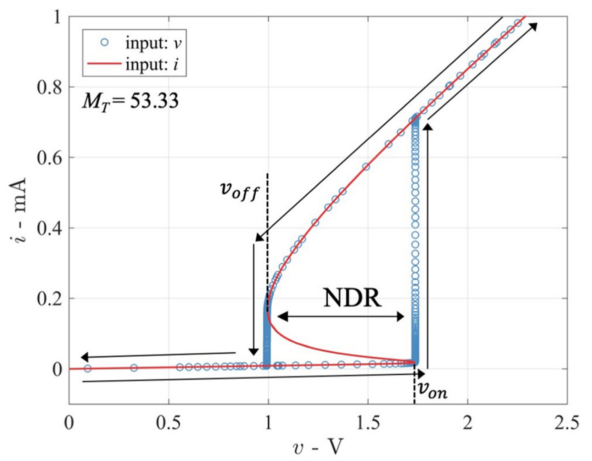

FIG. 1. Simulated quasi-static i–v curves for both voltage-controlled (blue circles) and current-controlled (red line) responses using the model and parameters introduced by Pickett and Williams.[14]

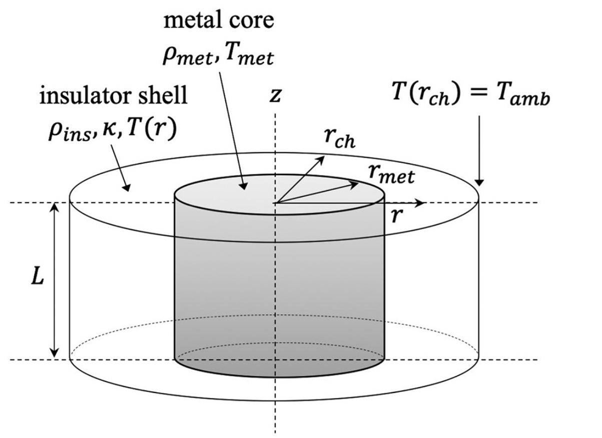

FIG. 2. Assumed geometry and boundary conditions.

find application for describing CC-NDR in Mott memristors constructed from other materials (e.g., VO_2[27] and TiO_2[1]) and in developing[27] and simulating[22,23] neuristor circuits for brain-like computing applications.

However, the equilibrium behaviors of this nonlinear state model for IMT induced threshold switching and their impacts on threshold switching, negative differential resistance, and current–voltage hysteresis remain under-explored, which limits the use of the model for designing devices to emulate plastic synapses and excitable neurons in neuromorphic circuitry. Particularly, the equilibrium states of this problem which determine the presence of CC-NDR have not been discussed.

Herein, we develop analytical expressions for the equilibrium states of Pickett and William's Mott memristor model and show that S-shaped NDR, and, thus, voltage-controlled (i.e., input: voltage, output: current) TS appears only above a critical ratio of insulator-to-metal resistivity, $M_c = e^2 + 1$. For ratios of resistivity below M_c, device resistance is nonlinear but also non-hysteretic. Above M_c, the voltage thresholds for reversible TS when operated as a voltage-controlled device increase in a nonlinear manner. This understanding enables tuning hysteresis in the i–v plane, features that benefit Mott memristors functioning as memory storage elements, as well as excitable devices mimicking neural action potentials.

For the reader's convenience, the equations defining the Mott memristor model established by Picket and Williams[14,20] are summarized here using the same notation. Per Chua's formulation of ideal memory resistance (memristance),[24] and consistent with the voltage-induced responses of NbO_2, Pickett and Williams proposed a nonlinear thermoelectrical model that couples the Joule-heating induced change in temperature of the material to a change in electrical resistance[14] and thus the resulting voltage or current that drive the rate of heating. The model states that the voltage, v, across the Mott memristor is related to the current, i, through it as given by

$$v = R_{ch}(u)i, \tag{1}$$

where R_{ch} is the total electrical resistance of a symmetric cylindrical channel (Fig. 2). The state variable, u, represents the ratio of the radius of the metallic portion, r_{met}, to the total channel radius, r_{ch}. For a current-controlled memristor, the rate of change of u is written as a function of device geometry, material parameters, and i. The nominal electrical resistance of the concentric channel accounts for parallel conduction pathways through both the insulating and metallic phases and is given by

$$R_{ch} = \frac{\rho_{ins} L}{\pi r_{ch}^2}\left[1 + \left(\frac{\rho_{ins}}{\rho_{met}} - 1\right)u^2\right]^{-1}, \tag{2}$$

where ρ_{ins} and ρ_{met} are values of resistivity of the insulating and metallic phases of the material, respectively, and L is the total length of the channel (i.e., distance between top and bottom electrodes). The dynamic thermal response of the concentric conductive channel is coupled to its electrical behavior by considering that the rate of Joule heating, P_{iv}, is equal to the rate at which heat conducts away from the metallic phase in a radial direction plus the rate of change in total enthalpy of the channel, ΔH, required for the insulator-to-metal Mott transformation, according to

$$P_{iv} = \Gamma_{th}(u)\Delta T + \frac{d\Delta H(u)}{dt}, \tag{3}$$

where the nominal thermal conductance, Γ_{th}, of an insulating shell with thermal conductivity, κ, in the radial direction is

$$\Gamma_{th}(u) = 2\pi L\kappa\left(\ln\frac{1}{u}\right)^{-1}, \tag{4}$$

and $\Delta T = T_{met} - T_{amb}$ is the maximum temperature difference between the uniform temperature of the metallic core, T_{met}, and the fixed ambient temperature, T_{amb}, at the boundary, $r = r_{ch}$. The temperature within the insulator decreases radially in a nonlinear fashion as given by

$$T(r) - T_{amb} = \begin{cases} \Delta T, & 0 < r < r_{met} \\ \Delta T \ln\left(\dfrac{r}{r_{ch}}\right)(\ln u)^{-1}, & r_{met} < r \le r_{ch}. \end{cases} \tag{5}$$

By the chain rule, the total time rate of change of enthalpy can be written as

$$\frac{d\Delta H(u)}{dt} = \frac{d\Delta H(u)}{du}\frac{du}{dt}, \tag{6}$$

where the change in enthalpy resulting from a variation in the radius of the metallic core, which is obtained from the sum of total heat capacity and the transformation enthalpy, is given by

$$\frac{d\Delta H(u)}{du} = \pi L r_{ch}^2\left[\hat{c}_p \Delta T \frac{1-u^2+2u^2\ln u}{2u(\ln u)^2} + 2\Delta\hat{h}_{tr} u\right]. \tag{7}$$

In this equation, $\hat{c}_p$ and $\Delta\hat{h}_{tr}$ are the heat capacity and enthalpy of transformation per unit volume, respectively, of the insulator material.

In terms of either applied current or voltage, the Joule heating power is given by

$$P_{iv} = \frac{v^2}{R_{ch}(u)} = i^2 R_{ch}(u). \tag{8}$$

Combining these expressions leads to ordinary differential equations for the state variable, u, either in terms of an input voltage, v,

$$\frac{du}{dt} = \left(\frac{d\Delta H(u)}{du}\right)^{-1}\left(\frac{v^2}{R_{ch}(u)} - \Gamma_{th}(u)\Delta T\right), \tag{9}$$

or applied current, i:

$$\frac{du}{dt} = \left(\frac{d\Delta H(u)}{du}\right)^{-1}\left(i^2 R_{ch}(u) - \Gamma_{th}(u)\Delta T\right). \tag{10}$$

The numerical integration of either Eq. (9) or Eq. (10) thus represents the dynamic evolution of the state variable u as a function of the applied stimulus.

In the supplementary material to Ref. 13, the Mott memristor model is defined by five equations, given here as (1), (2), (4), (7), and (10), which is the current-controlled formulation of the model. Alternatively, the model can be written in voltage-controlled form by replacing (10) by (9). For this study, the eight physical parameters in Table I, taken from Table S1 in Ref. 20, will be used.

The model implies that the temperature of the device will increase in response to either an applied voltage or an applied current.

TABLE I. Mott memristor physical parameters.

Symbol	Value	Unit	Remark
$\hat{c}_p$	2.6×10^6	J m^{-3} K^{-1}	Volumetric heat capacity
$\Delta\hat{h}_{tr}$	1.6×10^8	J m^{-3}	Volumetric enthalpy of transformation
κ	0.9	W m^{-1} K^{-1}	Thermal conductivity
ρ_{met}	3×10^{-4}	Ω m	Metallic phase electrical resistivity
ρ_{ins}	1.6×10^{-2}	Ω m	Insulating phase electrical resistivity
ΔT	784	K	Heating temperature
r_{ch}	30×10^{-9}	m	Conduction channel radius
L	20×10^{-9}	m	Conduction channel length

At a critical temperature change, ΔT, a portion of the insulator transforms to the metallic phase, which lowers both its electrical resistance and its ability to further heat up and alters the outward conduction of heat.

It is worth emphasizing that the physical meaning of u and the presence of natural logarithm, $\ln(u)$, constrain the state variable to remain strictly between 0 and 1. The model assumes axially symmetric behavior, uniformity of thermal and electrical properties along the length, and a response that is independent of the direction of current flow. Even though experimental data on niobium-dioxide from[14] reported threshold switching at only positive voltage, i–v symmetry is expected physically due to identical electrode chemistries and the independence of Joule heating on direction of current flow. The model captures the experimentally measured i–v behaviors exhibited in Mott memristors, in particular the hysteretic, resistive switching response to controlled voltage. What has not been discussed in the literature, however, is what are the conditions when NDR will be present in a device and at what voltages will hysteretic switching occur. Understanding this information is needed to unlock design of memristive devices that rely on these physics.

The equilibrium states of the model can be assessed by setting Eqs. (9) and (10) equal to zero and solving for v or i. Assuming a non-zero value of $\frac{d\Delta H(u)}{du}$, Eq. (9) yields the following set of equilibrium voltages v_{eq} where $v > 0$:

$$v_{eq} = \sqrt{R_{ch}(u)\Gamma_{th}(u)\Delta T} \quad \text{for } 0 < u < 1,$$

Similarly from Eq. (10), the set of equilibrium currents, i_{eq} where $i > 0$, are given by

$$i_{eq} = \sqrt{\frac{\Gamma_{th}(u)\Delta T}{R_{ch}(u)}} \quad \text{for } 0 < u < 1.$$

Figures 3(a) and 3(b) show equilibrium curves v_{eq} and i_{eq} (respectively) plotted vs u for different ratios of Mott transition insulator to metal resistivity, $M_T = \frac{\rho_{ins}}{\rho_{met}}$, where ρ_{met} and all other device parameters, except ρ_{ins}, are fixed at the values in Table I. The value $M_T = 53.33$ corresponds to the value of ρ_{ins} in the table. These equilibrium plots reveal several characteristics important for understanding the dynamic response of this nanodevice model.

Stability of an equilibrium state (u, v) on the curve v_{eq} (or (u, i) on i_{eq}) is indicated by the sign of the curve's slope at that point. A positive slope represents a stable state, whereas a negative slope indicates an unstable state. For example, v_{eq} in Fig. 3(a) for $M_T = 100$ shows an unstable region for $0.05 < u < 0.7$. Note that the plots of v_{eq} show that this type of instability appears as M_T increases from 2 to 15, whereas plots of i_{eq} display positive slopes across all values of M_T shown. These differences show that as u increases (upon Joule-heating induced Mott transformation), current equilibrium increases monotonically, but voltage equilibrium does not. Rather, v_{eq} displays a local maximum and local minimum as u increases for sufficiently large values of M_T.

As will be shown below, the presence or absence of hysteresis during dynamic simulations is directly related to the presence or absence of the unstable (negative slope) region of v_{eq} that arises as M_T passes through a critical value denoted by M_c. On the other hand, i_{eq} has a positive slope for all M_T. These two facts hold for the Mott

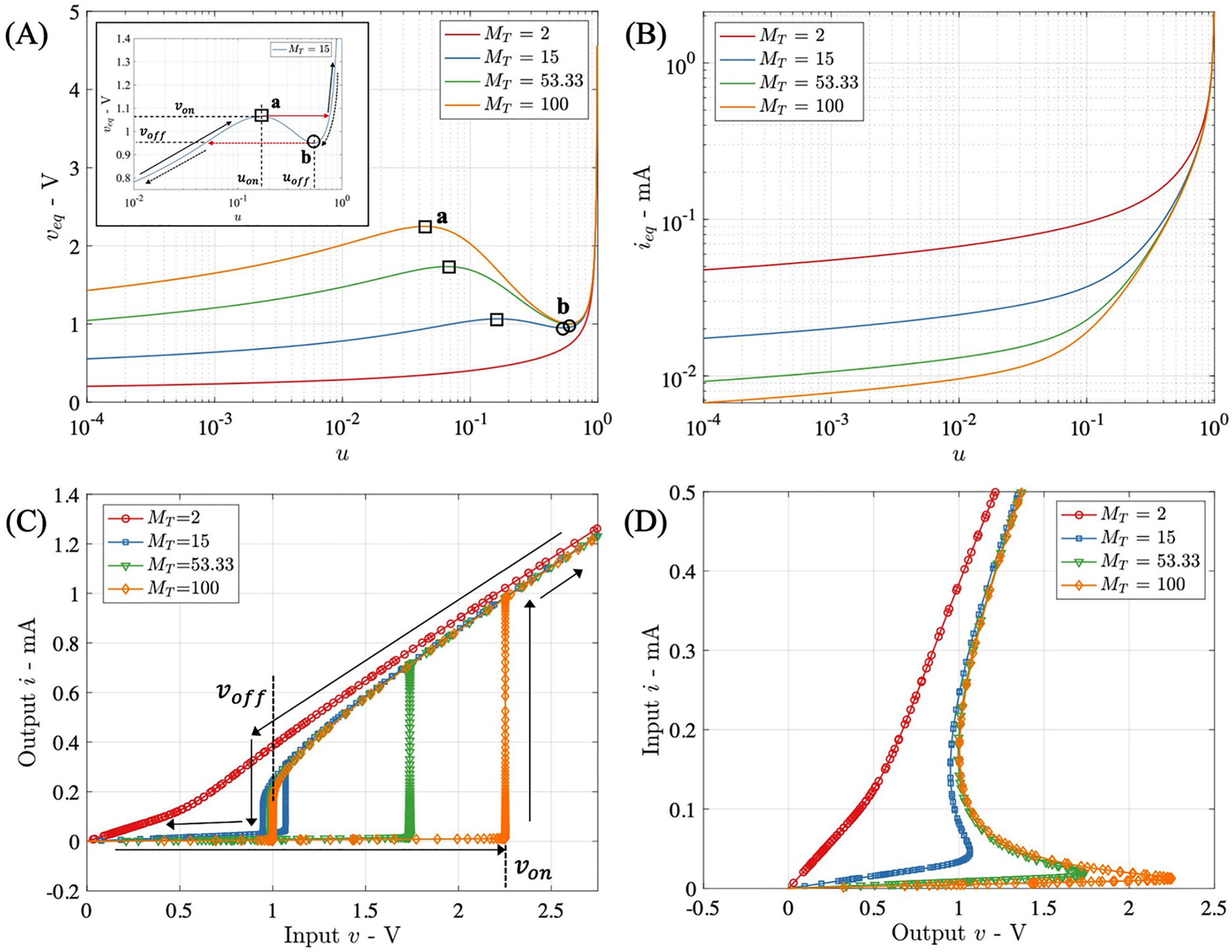

FIG. 3. Equilibrium (a) voltage and (b) current vs the state variable, u. Inset: a magnified view of the unstable $v_{eq} - u$ region for $M_T = 15$. The (u, v_{eq}) coordinates of **a** are (0.166 and 1.065), and those for **b** are (0.539 and 0.949). Simulated (c) voltage-controlled and (d) current-controlled quasi-static i–v relationships varying values of M_T. Arrows in (c) trace the current path vs voltage, and v_{on} and v_{off} labels represent switching thresholds.

memristor model regardless of the other physical parameters (such as κ) in the model.

The inset figure in the upper left of Fig. 3(a) shows a magnified view of these extrema, labeled **a** and **b**, for a single nonmonotonic equilibrium curve for $M_T = 15$. The solid black arrows show the trajectory of u as v_{eq} increases, while the dotted black arrows indicate the trajectory of u as v_{eq} decreases. The horizontal red arrow pointing to the right at **a** indicates that u snaps through from $\sim$0.166 to a value of $\sim$0.762 as v_{eq} rises above 1.065 V. This unstable increase in u when operated in a voltage-controlled manner is due to positive feedback that drives runaway heating and phase transformation: an increase in voltage increases heating power, which increases u, lowers R_{ch}, and further increases heating. The voltage where this occurs represents the threshold potential, v_{on}, for switching *on* the resistance from a high value at small u, often called R_{off}, to a much lower value, R_{on}, at large u. Further increases in v_{eq} correspond to stable growth of u. Once a device is in the *on* state, the radius of the metallic core is significantly larger, which means R_{ch} is relatively low. As a result, a voltage less than v_{on} can supply the same amount of heating power needed to maintain a stable fraction of metallic phase, u. Figure 3(a) shows that u stably drops until reaching a value of $\sim$0.54 at point **b**. Further reductions cause u to snap through to a significantly lower value of $\sim$0.048 (see leftward point red arrow), where this same value of voltage ($\sim$0.949 V) intersects the stable region of the curve to the left of **a**. This sudden decrease (and the corresponding rise in R_{ch}) sharply cuts the heating power at the same v. Thus, the transition from metallic phase to insulator phase is self-propelled too as v falls below v_{off}. The voltage at this transition represents the voltage threshold, v_{off}, for reverting the device from R_{on} to R_{off}. Figure 3(a) shows that both v_{on} and v_{off} increase for larger values of M_T.

Figures 3(c) and 3(d) show simulated i–v plots using either voltage-controlled [from Eq. (9)] or current-controlled [from Eq. (10)] versions of the model, respectively. In these plots, the controlled variable is labeled as the *input* on the axis label, while the dependent variable is labeled as the *output*. In Fig. 3(c), the response is nonlinear and non-hysteretic at $M_T = 2$. The maximum slope at higher voltages corresponds to the R_{on} value for the device when $u \rightarrow 1$ and channel resistance is dominated by the conductive metal core with substantial diameter. At higher values of M_T, responses become nonlinear and hysteretic, with sharp transitions (i.e., v_{on} and v_{off}) occurring between R_{off} (low current) and R_{on} (high current). Note that the high-current asymptote at large values of v (i.e., R_{on}) is the same in all cases because the value of ρ_{met} was fixed, while the value of ρ_{ins} was varied with M_T.

When current is controlled instead, Fig. 3(d) shows that i–v curves are nonlinear and also non-hysteretic for all values of M_T. The plot for $M_T = 2$ is identical to that predicted when voltage was controlled in Fig. 3(c). However, the i–v curves adopt an S-shape for values of $M_T \geq 15$ and include a region of NDR between the two locations of high curvature. Similar to the plot of $v_{eq} - u$ this nonlinear trend reveals the regions of stability and instability in the device: stable cases correspond to positive differential resistance (di/dv) seen at low and high values of current, whereas unstable regions correspond to the central region of negative differential resistance at intermediate values of current. The S-shape signifies that multiple values of current are possible for a particular controlled voltage (e.g., i could be <0.1 mA or >0.5 mA at $V = 1.5$ for $M_T = 100$), whereas there is only one possible value of voltage for a controlled level of current. This is the definition of current-controlled negative differential resistance (CC-NDR).

The existence of hysteresis can be determined from the voltage equilibrium curve by examining the zero-slope condition $dv_{eq}/du = 0$, resulting in the following equation:

$$Q(u) \equiv u^2(-2\ln u - 1) = (M_T - 1)^{-1}, \tag{11}$$

which involves only the ratio of resistivities, M_T. Figure 4(a) shows the function $Q(u)$ plotted as a black line. The colored horizontal lines represent different values for the right hand side of Eq. (11). Intersections between these colored lines and the black curve for Q, thus, depict the values of u where the slope of the $v_{eq} - u$ plot is zero, i.e., where TS occurs due to the instability in $v_{eq} - u$. In the case of $M_T = 2$, no intersection occurs, which verifies what is shown in Fig. 3(a) that no local extrema are present. The maximum value of Q is found to be $Q_c = e^{-2} \approx 0.135$, and it occurs at a critical value of the state variable $u_c = e^{-1} \approx 0.368$. This position sets the threshold for CC-NDR and TS in the model, where specifically $M_T > M_c = e^2 + 1 \approx 8.39$ for two intersections to occur between the left- and right-hand sides of Eq. (11). Hence, we see intersections present in the figure (marked by open squares and circles) for the three larger values of M_T, which are all greater than M_c. The blue markers for $M_T = 15$ correspond to the TS values of u for coordinates **a** and **b** in the inset in Fig. 3(a). The square marks when u snaps to the right as voltage increases (corresponding to v_{on}), whereas the circle marks when u snaps to the left as voltage decreases (corresponding to v_{off}). Physically, this analysis shows that in the model the relative resistivities of the insulating and metallic phases are the sole factor for determining whether $v_{eq} - u$ is N-shaped (i.e., whether CC-NDR is present), which allows for TS and i–v hysteresis in a voltage-controlled scenario.

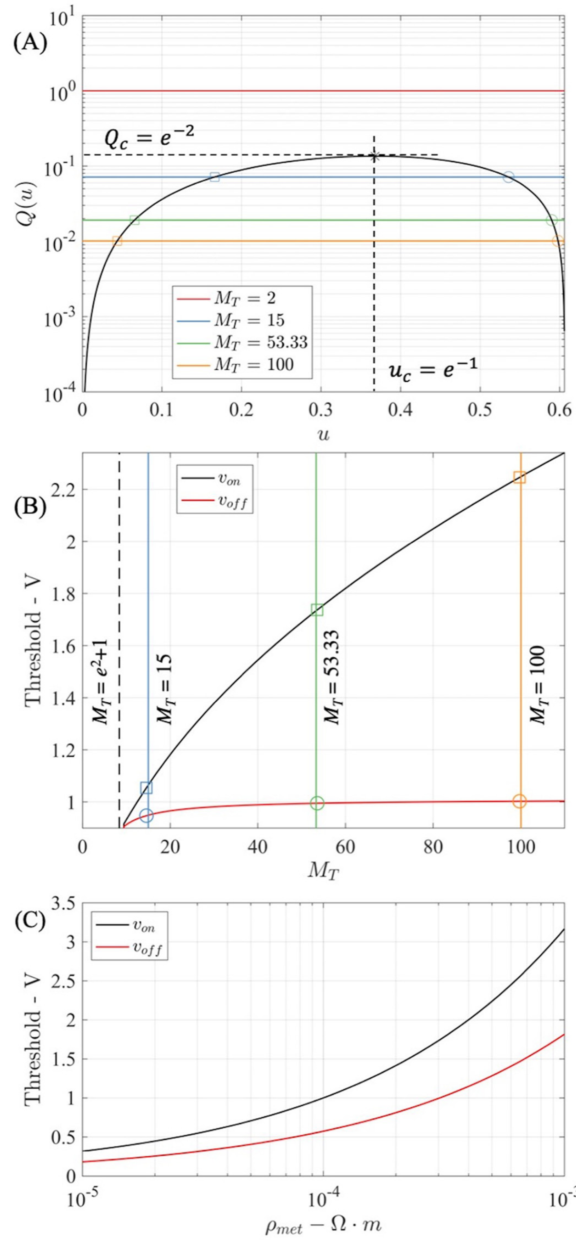

FIG. 4. (a) $Q(u)$ curve and its intersections with varying values of M_T. (b) Switching threshold voltages vs M_T during voltage-controlled for $\rho_{met} = 3 \times 10^{-4} \Omega$·m. Open squares and circles mark v_{on} and v_{off} thresholds, respectively. (c) Switching threshold voltages vs ρ_{met} for $M_T = \rho_{ins}/\rho_{met} = 53.33$.

Figure 4(b) reveals how the critical values of u corresponding to intersections of $Q(u)$ vs $(M_T - 1)^{-1}$ affect the switching thresholds identified as v_{on} and v_{off} for varying levels of M_T. Intersections for v_{on} (open squares) and v_{off} (open circles) at values of M_T used in Fig. 3 are also shown. The values of both thresholds increase in sublinear fashions with respect to M_T. Specifically, $v_{on} \propto\sim M_T^{0.3}$ for M_T near the critical value M_c and $v_{on} \propto\sim M_T^{0.5}$ for very large M_T, while v_{off}

saturates at a maximum value of $\approx$1.01 V. More simply, the plot reveals that large values of M_T result in substantial increases in the values of v_{on}, whereas v_{off} remains relatively fixed if ρ_{met} is fixed. The reason this transition converges to a near constant value of v_{off} for values of $M_T \gtrsim 15$ is because the electrical resistance of the metallic core, R_{met}, dominates when u is large. In this operating region, changing M_T does not significantly affect the current through the metallic core, which is the phase that governs the value of R_{ch} and sets the level of Joule heating. Additionally, Fig. 4(c) shows that a higher nominal value of ρ_{met} also translates into higher values of v_{on} and v_{off}. Alternatively, increasing M_T by lowering ρ_{met} relative to a fixed value of ρ_{ins} results in sublinear reductions in both v_{on} and v_{off} with increasing values of M_T.

Examination of the current equilibrium curve via the zero-slope condition $di_{eq}/du = 0$ yields the following equation:

$$u^2(2\ln u - 1) = (M_T - 1)^{-1}, \tag{12}$$

which differs from Eq. (11) only by changing the sign of the natural logarithm term. Since the left-hand side of Eq. (12) is negative for $0 < u < 1$, there are no physically valid solutions. In other words, the slope of the current equilibrium curve is positive for all $M_T > 0$ and it yields no new information, in contrast to the voltage equilibrium curve.

In this Letter, we revealed the criterion for TS and CC-NDR in the Mott memristor model through equilibrium analysis: M_T, the ratio of insulator to metallic resistivities, must be larger than a critical value, $M_c = e^2 + 1 \approx 8.39$, corresponding to a critical value for the metallic fraction, $u_c = e^{-1}$. Physically, this criterion implies that when the drop in device resistance is too small, the subsequent increase in current is not sufficient to raise the temperature above the Mott transition. Below M_c, v_{eq} increases monotonically with increasing u; thus, the device cannot exhibit NDR or TS since v_{eq} is stably maintained across the full range of u. Above this onset value, however, we demonstrated that $v_{eq} - u$ is N-shaped in its trajectory, with a central region where v_{eq} decreases unstably with increasing values of u. The local maximum and minimum values of v_{eq} in this curve define the limits of u where NDR is present, and their magnitudes represent critical voltages where TS occurs by using the $v_{eq} - u$ relationship. Above M_c, the threshold voltages increase in sublinear fashions with rising values of M_T. In contrast, $i_{eq} - u$ increases monotonically with u regardless of the value M_T. This trend masks the dependence of NDR on a minimum value of M_T, even though simulated i–v in a current-operated mode clearly shows that S-shaped NDR appears only for cases when $M_T > M_c$.

The physical model in study is framed as a dynamic memristive model that is based on a geometrically simplified system and which uses a single state variable, u. Equations (9) and (10) show that the dynamic state equation for u can be written either in terms of v or i, as a way to recreate what may be observed in a measurement. These differential equations are nonlinear and inherently stiff in the sense of Curtis and Hirschfelder.[28] Therefore, simulations using them benefit from an appropriate ode solver (e.g., *ode23tb* in MATLAB). Additionally, the reader should note that the equilibrium states of the model correspond to Curtis and Hirschfelder's "pseudo-stationary" solutions.[28] Our simulations of quasi-static i–v were obtained by inputting sufficiently slow waveforms. For the physical parameters in Table I, we found that a 10 kHz frequency exhibited quasi-static behaviors, seen in Figs. 1 and 3(c) as vertical changes in i at the threshold voltages. Increasing the sweep rate introduces dynamics into the i–v responses that shift the apparent thresholds for TS.

Our analysis reveals the importance of the insulator-metallic resistivity in determining whether NDR and TS occur, and it provides new insights into how the threshold voltages (i.e., v_{on} and v_{off}) vary. Enabling a direct route to controlling these thresholds has practical value since voltage-controlled TS devices are candidate building blocks for neural network-based computing: for analog vector-matrix multiplication acceleration in artificial neural networks, and in hardware-based spiking neural networks. Decreasing the values of v_{on} and v_{off} lowers the power required to adjust device conductance and enables shaping of the generated spikes. Therefore, we propose the findings of this work can be used to help design the switching characteristics and resistance values of the devices, through both material selection and device geometry.

S.A.S. acknowledges support from Air Force Office of Scientific Research Grant No. FA9550-19-1-0213. J.S.P. would like to thank Professor Walter Lacarbonara from Sapienza University of Rome, Italy, for the introduction leading to this work.

DATA AVAILABILITY

Data sharing is not applicable to this article as no new data were created or analyzed in this study.

REFERENCES

[1] Y. Dai, F. Tao, and M. Qi, J. Appl. Phys. **126**, 075705 (2019).
[2] Y. Liang, G. Wang, G. Chen, Y. Dong, D. Yu, and H. H. C. Iu, IEEE Trans. Circuits Syst. I **67**, 5139 (2020).
[3] I. Messaris, R. Tetzlaff, A. Ascoli, R. S. Williams, S. Kumar, and L. Chua, "A simplified model for a NbO_2 Mtt memristor physical realization," in *2020 IEEE International Symposium on Circuits and Systems (ISCAS)*, 2020.
[4] S. Kumar, Z. Wang, N. Davila, N. Kumari, K. J. Norris, X. Huang, J. P. Strachan, D. Vine, A. D. Kilcoyne, and Y. Nishi, Nat. Commun. **8**, 658 (2017).
[5] S. Slesazeck, H. Mähne, H. Wylezich, A. Wachowiak, J. Radhakrishnan, A. Ascoli, R. Tetzlaff, and T. Mikolajick, RSC Adv. **5**, 102318 (2015).
[6] Y. Kalcheim, A. Camjayi, J. del Valle, P. Salev, M. Rozenberg, and I. K. Schuller, Nat. Commun. **11**, 2985 (2020).
[7] X. Liu, S. Li, S. K. Nandi, D. K. Venkatachalam, and R. G. Elliman, J. Appl. Phys. **120**, 124102 (2016).
[8] R. Tobe, M. S. Mian, and K. Okimura, J. Appl. Phys. **127**, 195103 (2020).
[9] M. Pattanayak, M. N. F. Hoque, Y. Zhao, Z. Fan, and A. A. Bernussi, Semicond. Sci. Technol. **34**, 105028 (2019).
[10] H.-T. Kim, B.-J. Kim, S. Choi, B.-G. Chae, Y. W. Lee, T. Driscoll, M. M. Qazilbash, and D. N. Basov, J. Appl. Phys. **107**, 023702 (2010).
[11] P. Maffezzoni, L. Daniel, N. Shukla, S. Datta, and A. Raychowdhury, IEEE Trans. Circuits Syst. I **62**, 2207 (2015).
[12] M. Pattanayak, M. N. F. Hoque, Z. Fan, and A. A. Bernussi, Sci. Technol. Adv. Mater. **19**, 693 (2018).
[13] M. D. Pickett and R. S. Williams, Nanotechnology **24**, 384002 (2013).
[14] M. D. Pickett and R. S. Williams, Nanotechnology **23**, 215202 (2012).
[15] L. O. Chua, Int. J. Bifurcation Chaos **15**, 3435 (2005).
[16] T. Hennen, D. Bedau, J. A. J. Rupp, C. Funck, S. Menzel, M. Grobis, R. Waser, and D. J. Wouters, "Forming-free Mott-oxide threshold selector nanodevice showing s-type NDR with high endurance (>1012 cycles), excellent Vth stability (5%), fast (<10 ns) switching, and promising scaling properties," in *2018 IEEE International Electron Devices Meeting (IEDM)* (IEEE, 2018), pp. 37.5.1–37.5.4.
[17] N. K. Upadhyay, H. Jiang, Z. Wang, S. Asapu, Q. Xia, and J. Joshua Yang, Adv. Mater. Technol. **4**, 1800589 (2019).
[18] J. del Valle, P. Salev, Y. Kalcheim, and I. K. Schuller, Sci. Rep. **10**, 4292 (2020).
[19] M. S. Feali, A. Ahmadi, and M. Hayati, Neurocomputing **309**, 157 (2018).

[20]M. D. Pickett, G. Medeiros-Ribeiro, and R. S. Williams, Nat. Mater. **12**, 114 (2013).
[21]S. Kumar, J. P. Strachan, and R. S. Williams, Nature **548**, 318 (2017).
[22]Y. Bo, P. Zhang, Y. Zhang, J. Song, S. Li, and X. Liu, J. Appl. Phys. **127**, 245101 (2020).
[23]Y. Bo, P. Zhang, Z. Luo, S. Li, J. Song, and X. Liu, Adv. Intell. Syst. **2**, 2000066 (2020).
[24]L. O. Chua and K. S. Mo, Proc. IEEE **64**, 209 (1976).
[25]L. Chua, IEEE Trans. Circuit Theory **18**, 507 (1971).
[26]L. Chua, Semicond. Sci. Technol. **29**, 104001 (2014).
[27]W. Yi, K. K. Tsang, S. K. Lam, X. Bai, J. A. Crowell, and E. A. Flores, Nat. Commun. **9**, 4661–30405124 (2018).
[28]C. F. Curtiss and J. O. Hirschfelder, Proc. Natl. Acad. Sci. U. S. A. **38**, 235 (1952).